Micro-CT Analysis of Rodent Temporal Bones: Identifying Optimal Species for Otological Research

Hannah Daoudi, Evelyne Ferrary, Cerine Moula, Florence Agnely, Amélie Bochot, Catherine Cailleau, Yann Nguyen, Ghizlène Lahlou, Renato Torres

Laryngoscope Investigative Otolaryngology

Laryngoscope Investigative Otolaryngology

ORIGINAL RESEARCH OPEN ACCESS

Micro-CT Analysis of Rodent Temporal Bones: Identifying Optimal Species for Otological Research

Hannah Daoudi[1,2] | Evelyne Ferrary[1,2] | Cerine Moula[3] | Florence Agnely[3] | Amélie Bochot[3] | Catherine Cailleau[3] | Yann Nguyen[1,2] | Ghizlène Lahlou[1,2] | Renato Torres[1,2]

[1]Université Paris Cité, Institut Pasteur, AP-HP, Inserm, Fondation Pour l'audition, Institut de l'audition, IHU Re-Connect F-75012, Technologies and Gene Therapy for Deafness, Paris, France | [2]ENT Department, Pitié-Salpêtrière, APHP, Sorbonne University, Paris, France | [3]Paris-Saclay University, CNRS, Galien Paris-Saclay Institute, Orsay, France

Correspondence: Hannah Daoudi (hannah.daoudi@aphp.fr)

Received: 18 February 2025 | **Revised:** 12 May 2025 | **Accepted:** 11 June 2025

Funding: We thank Fondation Pour l'Audition (starting grant IDA-2020, FPARD-2022-09). This work has been benefited from a French government grant managed by the Agence Nationale de la Recherche and the France 2030 program, reference ANR-23-IAHU-0003, and Agence Nationale de la Recherche TympaBiOM ANR-22-CE52-0006. H.D. received financial aid through an interface contract from the Institut Pasteur.

Keywords: animal model | cochlea | imaging | middle ear anatomy | three-dimensional anatomy

ABSTRACT

Objectives: Rodents are used in most otological research studies and the choice of the most appropriate animal model may be crucial in studies of ear diseases and in the development of effective treatments. Here, we used micro-CT to compare temporal bone anatomy between four rodent model animals (guinea pigs, gerbils, rats, and mice) and humans, aiming to better characterize the anatomy of the inner and middle ear, and facial nerve to support informed animal model selection in otologic research.

Methods: We generated three-dimensional reconstructions and measured the various middle (tympanic membrane, ossicular chain, and facial nerve) and inner (cochlea, vestibular labyrinth) ear structures.

Results: Each structure of the middle or inner ear of each rodent was described and measured.

Conclusion: This micro-CT analysis of rodents can guide researchers in their choice of the most suitable middle or inner ear models based on the specific anatomic area of interest. Our findings highlight the strengths and limitations of each species, providing essential insight that could enhance the precision and applicability of otological studies.

Level of Evidence: 4.

1 | Introduction

Choosing the relevant animal model is crucial for studying ear diseases and effective volume-adapted treatments. Most otological research involves rodents from two families—*Muridae* (gerbils, rats, and mice) and *Caviidae* (guinea pigs)—due to the physiological and anatomical resemblances between the ears of these animals and those of humans [1, 2]. Each species has particular advantages and challenges, and selecting the most appropriate model is a critical decision. Given the small size and delicate structure of the ear, this choice can significantly affect the feasibility of accessing key anatomical structures, such as the tympanic membrane, ossicular chain, cochlea, or facial nerve, and the translatability of experimental procedures to human conditions. Nevertheless, few studies have analyzed rodent ear structures specifically in the context of their relevance to human otological research [1, 3–6]. We need to close this gap in our knowledge to ensure the selection of the most appropriate rodent models for addressing the objectives of particular studies, according to the organ of interest.

Anatomic dissection procedures have frequently been used in studies of the morphology of the middle and inner ear [1, 5, 7]. However, these methods are time-consuming and may not necessarily provide a global comprehensive three-dimensional (3D) anatomical representation. Scanning electron microscopy has also been widely used for the detailed imaging of ear structures. However, this approach requires prior dissection of the ear and can only be performed on a small sample from the animal organ [1]. It can also damage some anatomical structures.

In recent years, high-resolution micro-computed tomography (micro-CT) has emerged as a source of innovation for ex vivo and in vivo imaging, providing a high-resolution image without the need for the prior dissection of specimens, facilitating faster analyses, and specimen reuse. For the temporal bone in particular, this advanced imaging technique enables researchers to visualize the delicate structures with unparalleled clarity and precision, bridging significant gaps in our understanding of ear anatomy and pathology [8].

In this study, we used micro-CT analysis to determine the most suitable rodent species for otological research. We aimed to compare the anatomy of the middle and inner ear, and of the facial nerve, between rodent species and between rodents and humans.

2 | Material and Methods

2.1 | Human Cadaveric Bones

Four thawed cadaveric temporal bones from separate donors were used (Science Care, Phoenix, AZ, USA): two from the right side and two from the left side. The use of human temporal bones was authorized for scientific purposes by the French Ministry of Education, Research and Innovation (#IE20211231). The samples were purchased already sectioned; we only reduced their size so they would fit into the micro-CT scanner (less than 7 cm in length).

2.2 | Animals

We studied both ears of thawed adult rodent cadavers following the completion of ethically approved animal research unrelated to the ear and approved by the French Ethics Committee. We used two male Hartley guinea pigs (Charles River France, Domaine des Oncins, L'Arbresle, France), one male and one female Mongolian gerbil (Janvier Laboratories, Le Genest-Saint-Isle, France), two male Sprague Dawley rats (Janvier Laboratories, Le Genest-Saint-Isle, France), and one male and one female C57BL/6 mouse (Janvier Laboratories, Le Genest-Saint-Isle, France).

2.3 | Imaging Technique

All human temporal bones and animal heads were used for micro-CT scanning (Quantum FX, PerlinElmer, Massachusetts, USA). The scanning parameters were as follows:

- For the human cadaveric temporal bones: A field of view (FOV) of 30 mm (scan volume), with a spatial resolution of 59 μm (voxel size), at 90 kVp and 160 μA, over an acquisition time of 3 min.
- For mice: FOV of 10 mm, resolution of 20 μm, at 90 kVp and 160 μA, 3 min.
- For gerbils: FOV of 20 mm, resolution of 40 μm, at 90 kVp and 160 μA, 2 min.
- For guinea pigs and rats: FOV of 30 mm, resolution of 59 μm, at 90 kVp and 160 μA, 3 min.

Micro-CT scanning generated a high-resolution 3D volume that could be sliced digitally in any orientation.

2.4 | Image Analysis

Image analysis was conducted by two otologists (H.D. and R.T.) with the 3D multiplanar reconstruction viewer of the General Public License software Horos v.3.3.6 (Horos project, Geneva, Switzerland). Care was taken to ensure that each measurement was performed at the same location for all animal species. The analysis proceeded as follows:

- The axial plane was aligned with the lateral semicircular canal axis (Figure 1A). The lateral external ear canal diameter, the tympanic membrane diameter, the lateral semicircular canal diameter and the facial nerve diameter (second portion) were measured. On a coronal plane intersecting with the umbo of the malleus, diameters of the lateral external ear canal and the tympanic membrane were also measured (Figure 1A).
- The incudo-malleolar complex was aligned by ensuring that the coronal and axial planes intersected with the complex axis. The lengths of the incudo-malleolar complex, malleus, and incus were measured (Figure 2A).
- The orientation of the stapes was established by aligning the coronal and sagittal planes with the stapes axis. We measured the height and width of the stapes, the length and width of the footplate, and the width of each crura (Figure 2A).
- For cochlear analysis, the axial plane was aligned with the middle plane of the basal turn. The sagittal plane was matched with the middle of the basal turn, and the coronal plane intersected with the center of the round window and the cochlear turn at 180°. We measured the distance from the center of the round window to the lateral wall at 180° on the coronal plane (Distance A), the height of the cochlea at the apical turn from the base to its highest point on the sagittal plane (Distance H), and the diameters of the round window and the cochlea nerve (Figure 3A).

2.5 | 3D Reconstruction

We generated 3D reconstruction models using ITK-SNAP 3.4.0 (US National Institutes of Health) for semi-automated

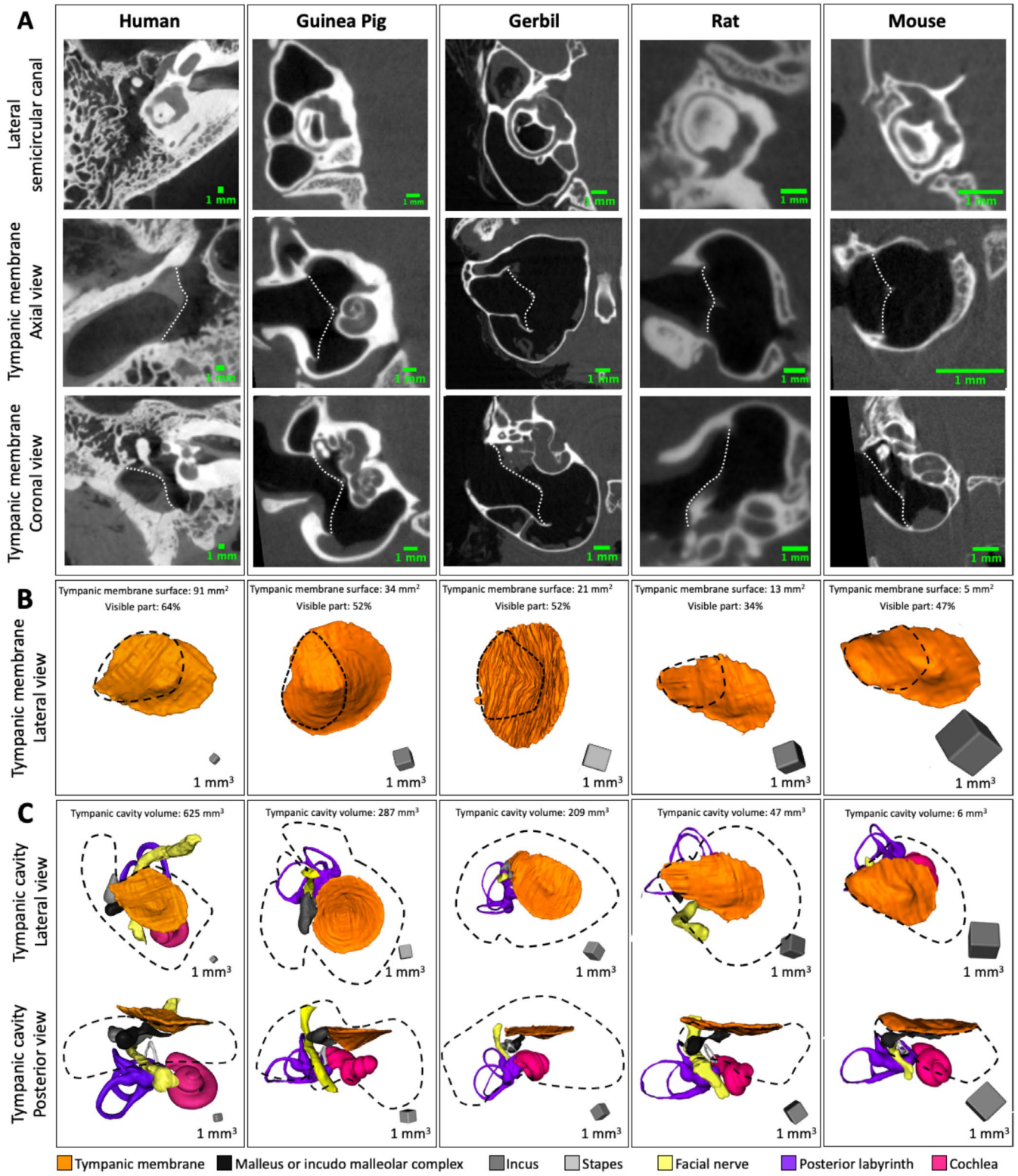

FIGURE 1 | Tympanic membrane and cavity in humans and rodents. Micro-CT views of a right ear (A). The axis of the axial plane was aligned with respect to the lateral semicircular canal (upper image). The tympanic membrane (dotted line) was measured on the axial plane (middle image), and the coronal plane passing through the umbo (lower image). 3D reconstruction of the tympanic membrane (B). The dotted line delimits the part of the membrane visible via the external auditory canal. 3D reconstruction of the middle and inner ear, lateral (upper image) and posterior (lower image) views (C). The dotted line delimits the tympanic cavity.

segmentation, and visualized the resulting structures with CloudCompare (v2.10.2). One right ear per species was selected for this process. The segmentation was performed under continuous visual control to ensure accurate delineation of each anatomical boundary. 3D reconstructions were obtained for the middle ear (tympanic membrane, malleus, incus, and stapes),

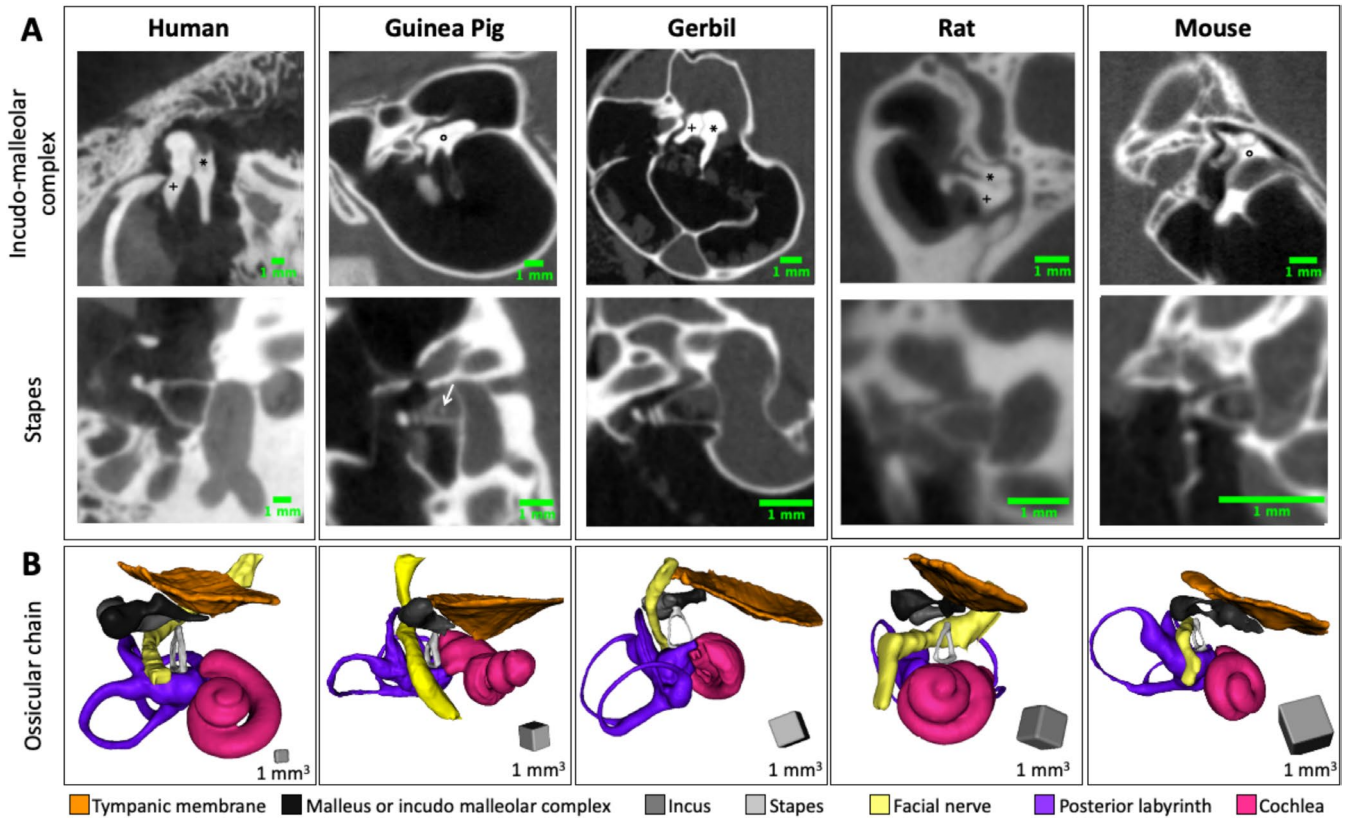

FIGURE 2 | Ossicular chain of humans and rodents. Micro-CT views of a right ear (A). View of the incudo-malleolar complex (⁺malleus, *incus, ◦incudo-malleolar complex) along a sagittal plane aligned with its axis (upper image). View of the stapes along an axial plane aligned with its axis (lower image). In the image for the guinea pig, the crista stapedius is indicated by the white arrow. 3D reconstruction of the middle and inner ears, ossicular chain view (B).

the inner ear (cochlea and vestibular labyrinth), the facial nerve, and the tympanic cavity. The segmentation software quantified the number of included voxels and converted this into surface area (mm^2) and volume (mm^3) measurements. We computed the area of the tympanic membrane and the stapes footplate, as well as the volume of each ossicle (malleus, incus, and stapes), the cochlea, the vestibular labyrinth, and the tympanic cavity (after exclusion of ossicular volumes).

The access to the tympanic membrane though the external auditory canal was calculated as the percentage of the accessible tympanic membrane surface to the total tympanic membrane surface. The ratio of the tympanic membrane and stapes footplate areas was calculated as follows: $\frac{\text{tympanic membrane area}}{\text{stapes footplate area}}$. The ratio of the volumes of the tympanic cavity and the ossicular chain was calculated as follows: $\frac{\text{tympanic cavity volume}}{\text{malleus} + \text{incus} + \text{stapes volume}}$.

2.6 | Statistical Analysis

The results are presented as the mean ± standard deviation (SD). A two-way ANOVA with Tukey multiple comparisons test was conducted on 19 morphometric parameters obtained from the four species (guinea pig, gerbil, rat, and mouse) to assess interspecies anatomical variation.

3 | Results

3.1 | External Auditory Canal

In humans, the mean diameter of the external auditory canal (anteroposterior × Inferior–superior) was 5.3 × 7.4 mm (Table 1). In guinea pigs, this diameter was 2.7 × 2.2 mm, corresponding to the largest opening in rodents, while gerbils, rats, and mice all displayed smaller canals, measuring less than 2 mm (Figure S1).

3.2 | Tympanic Membrane

The area and diameter of the tympanic membrane are reported in Table 1. The tympanic membrane had an area of 91 mm^2 in humans. In rodents, tympanic membrane area was greatest for guinea pigs (34 mm^2), followed by gerbils (21 mm^2) and rats (13 mm^2). Mice had the smallest tympanic membrane, with a surface area of only 5 mm^2. Access to the tympanic membrane was more limited in rodents than in humans, due to the external auditory canal providing visibility for only the upper half of the tympanic membrane (Figure 1B). The proportion of the tympanic membrane visible via the external auditory canal was 64% for humans, 52% for guinea pigs and gerbils, 47% for mice and only 35% for rats.

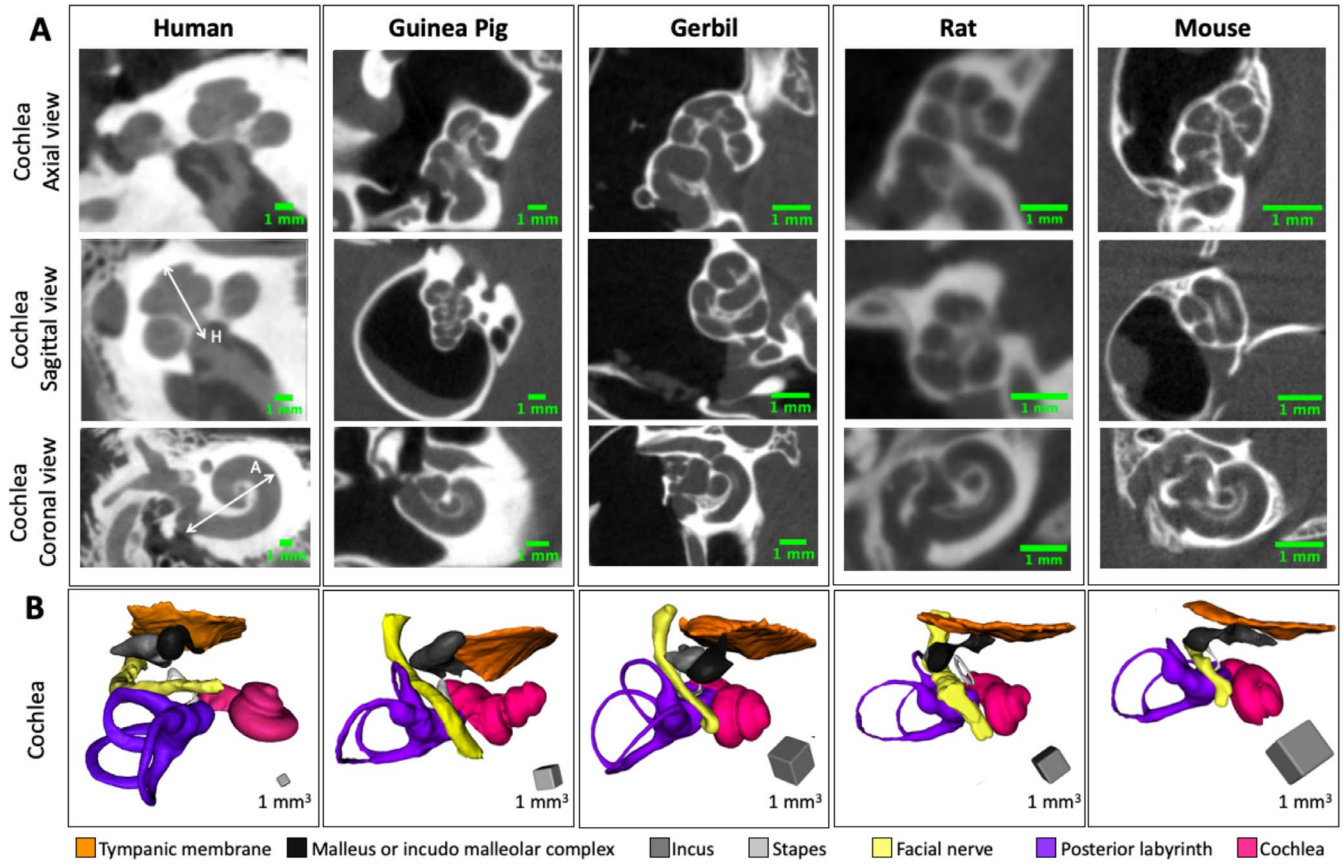

FIGURE 3 | Cochlea of humans and rodents. Micro-CT views of a right ear (A). The axial plane was aligned with the middle plane of the basal turn (upper image). The sagittal plane was aligned with the basal turn (middle image). The height of the cochlea was measured on this plane (double arrow, H). The coronal plane intersected with the center of the round window and the cochlear turn at 180° (lower image). Distance A was measured on this plane (double arrow, A). 3D reconstruction of the middle and inner ears, cochlear view (B).

3.3 | Tympanic Cavity

The volume of the tympanic cavity was generally proportional to animal size, with humans showing the largest volume (625 mm^3), followed by guinea pigs (287 mm^3) (Table 1, Figure 1C). Interestingly, gerbils exhibited a larger tympanic cavity (209 mm^3) than rats (47 mm^3), despite their smaller body size. This finding highlights a species-specific anatomical feature that may influence middle ear mechanics. Mice had the smallest tympanic cavity volume (6.4 mm^3), reflecting their overall smaller anatomy.

3.4 | Incudo-Malleolar Complex

In humans, gerbils, and rats, the incus and malleus are separate articulated entities, whereas in guinea pigs and mice they are fused, forming the incudo-malleolar complex. The volume of the complex ranges from 0.4 to 2.8 mm^3 in rodents, versus 29 mm^3 in humans (Table 1, Figure 2).

3.5 | Stapes

The human stapes has two crura and an involuted stapedial artery. By contrast, in guinea pigs, the crista stapedius, a bony bridge corresponding to the calcified remnants of the stapedial artery, passes between the crura [3]. In gerbils, rats, and mice, the carotid artery was found to pass between the crura of the stapes (Figure 2A), as in previous studies [5, 9], decreasing maneuverability. The height of the stapes was 3.7 ± 0.11 mm for humans. The stapes height was significantly greater in guinea pigs (1.6 ± 0.00 mm) compared to gerbils (1.4 ± 0.00 mm, $p = 0.048$) and rats (1.3 ± 0.03 mm, $p = 0.0007$), which displayed no significant difference between each other (NS, Two-way ANOVA, see Figure S1). The smallest height was observed in mice (0.7 ± 0.05 mm), showing a marked difference from all other species ($p < 0.0001$, Two-way ANOVA, see Figure S1 and Table 1).

Finally, the ratio of the areas of the stapes footplate and the tympanic membrane was 30 for humans. A similar value (about 38) was obtained for mice, whereas this ratio was higher (~50) in guinea pigs, gerbils and rats, suggesting a greater amplification of the sound waves transmitted from the tympanic membrane to the footplate (Table 1).

3.6 | Cochlea

In rodents, cochlear morphology varies between species, with differences in the number of turns: with 2.5 turns in humans, 3.5 in guinea pigs, 3 in gerbils, 2.5 in rats, and 2 in mice (Table 1). A knowledge of intracochlear volume is crucial for intra-labyrinthine therapeutic approaches. Guinea pigs have the largest cochlear volume (11 mm^3). Gerbils and rats have

TABLE 1 | Comparative analysis of ear measurements obtained by micro-CT imaging for humans and four rodent species.

	Human ($n=4$)	Guinea pig ($n=3$)	Gerbil ($n=4$)	Rat ($n=4$)	Mouse ($n=4$)
Approximate weight	70 kg	400 g	80 g	300 g	30 g
External auditory canal					
Diameter (mm)					
Anteroposterior	5.3 ± 0.51	2.7 ± 0.10	2.0 ± 0.10	1.4 ± 0.12	1.4 ± 0.11
Inferior–superior	7.4 ± 0.58	2.2 ± 0.30	1.8 ± 0.13	2.0 ± 0.12	1.7 ± 0.07
Tympanic membrane					
Diameter (mm)					
Anteroposterior	10.2 ± 0.66	6.8 ± 0.15	4.1 ± 0.29	3.0 ± 0.10	1.9 ± 0.10
Inferior–superior	11.3 ± 0.66	6.4 ± 0.10	6.0 ± 0.17	4.3 ± 0.30	3.1 ± 0.08
Area (mm^2)	91	34	21	13	5.4
Proportion of area visible (%)	64%	52%	52%	34%	47%
Tympanic cavity					
Volume (mm^3)	625	287	209	47	6.4
Tympanic cavity/ossicular chain ratio	20	98	170	65	13
Ossicular chain					
Malleus and incus					
Separate?	Yes	No	Yes	Yes	No
Length (mm)					
Incudo malleolar complex	3.5 ± 0.40	3.0 ± 0.10	1.7 ± 0.22	1.5 ± 0.05	0.9 ± 0.07
Malleus	6.9 ± 0.68	1.5 ± 0.06	1.9 ± 0.08	2.0 ± 0.06	1.5 ± 0.06
Incus	6.4 ± 0.26	1.8 ± 0.08	1.3 ± 0.10	1.4 ± 0.06	0.8 ± 0.03
Volume (mm^3)					
Malleus	13.0	2.8	0.7	0.4	0.4
Incus	15.6		0.45	0.24	
Stapes					
Height (mm)	3.7 ± 0.11	1.6 ± 0.00	1.4 ± 0.00	1.3 ± 0.03	0.7 ± 0.05
Width (mm)	2.6 ± 0.23	1.2 ± 0.03	0.9 ± 0.00	0.7 ± 0.08	0.4 ± 0.03
Anterior crus width (mm)	0.22 ± 0.04	0.13 ± 0.036	0.08 ± 0.012	0.09 ± 0.007	0.04 ± 0.007
Posterior crus width (mm)	0.26 ± 0.02	0.14 ± 0.038	0.09 ± 0.011	0.10 ± 0.019	0.16 ± 0.23
Volume (mm^3)	1.90	0.13	0.08	0.08	0.09
Footplate					
Length (mm)	2.4 ± 0.17	1.1 ± 0.06	0.9 ± 0.10	0.7 ± 0.09	0.4 ± 0.04
Width (mm)	0.25 ± 0.04	0.09 ± 0.005	0.09 ± 0.011	0.09 ± 0.007	0.06 ± 0.009
Area (mm^2)	3.10	0.67	0.39	0.27	0.14
Tympanic membrane/ footplate area ratio	30	51	55	47	38
Internal carotid artery[a]	No	Crista stapedius	Yes	Yes	Yes

(Continues)

TABLE 1 | (Continued)

	Human ($n=4$)	Guinea pig ($n=3$)	Gerbil ($n=4$)	Rat ($n=4$)	Mouse ($n=4$)
Cochlea					
Number or turns	2.5	3.5	3	2.5	2
Height (mm)	4.0 ± 0.17	3.5 ± 0.26	1.9 ± 0.10	1.9 ± 0.06	1.1 ± 0.03
Distance A[b] (mm)	9.1 ± 0.35	3.7 ± 0.06	2.5 ± 0.12	2.8 ± 0.10	1.7 ± 0.02
Volume (mm^3)	78	11	4.9	3.7	1.08
Round window diameter (mm)	1.6 ± 0.07	0.8 ± 0.05	0.6 ± 0.05	0.7 ± 0.10	0.3 ± 0.02
Cochlear nerve diameter (mm)	2.3 ± 0.05	0.8 ± 0.05	0.5 ± 0.05	0.6 ± 0.05	0.5 ± 0.09
Posterior labyrinth					
Canal diameter (mm)	1.2 ± 0.08	0.3 ± 0.06	0.2 ± 0.01	0.2 ± 0.01	0.1 ± 0.02
Volume (mm^3)					
Semicircular canals	58.1	4.9	1.8	1.6	0.6
Vestibule	31.9	5.9	2.1	1.9	0.49
Total inner ear volume	168	22	8.8	7.2	2.2
Facial nerve					
Diameter (mm)	1.4 ± 0.15	0.3 ± 0.06	0.4 ± 0.03	0.6 ± 0.06	0.2 ± 0.02

Note: The data shown are the mean ± standard deviation. For volume measurements, the mean and standard deviation are not provided, as they were calculated from 3D reconstruction models based on a single right ear per species. Distances are expressed in mm, areas in mm^2 and volumes in mm^3.
[a]The internal carotid artery passes between the cura of the stapes in gerbils, rats, and mice.
[b]Distance A is measured as the distance from the center of the round window to the lateral wall at 180° on a coronal plane passing through the round window and the basal turn of the cochlea.

relatively similar cochlear volumes (4.9 and 3.7 mm^3, respectively), whereas mice have a much smaller cochlear volume (1.08 mm^3) (Table 1, Figure 3). Finally, the diameter of the round window in guinea pigs, gerbils, and rats (0.8 ± 0.05, 0.6 ± 0.05, and 0.7 ± 0.10 mm, respectively) is sufficiently large for the insertion of a cochlear implant (these implants having a diameter of about 0.6 mm) whereas that of mice is too small (round window diameter of 0.3 mm) for implant insertion.

3.7 | Vestibular Labyrinth

Vestibular volume ranged from 0.5 to 6 mm^3 in rodents, and semicircular canal volume from 0.6 to 5 mm^3 (Table 1, Figure 4). The canal diameter was quite similar among rodents and ranged from 0.1 to 0.3 mm, but much smaller than that of humans (1.2 ± 0.08 mm) (Figure S1).

3.8 | Facial Nerve

The diameter of the facial nerve varied among rodent from 0.2 to 0.6 mm in rodents, compared to 1.4 ± 0.15 mm in humans (Table 1).

4 | Discussion

We did not aim here to establish a precise anatomical atlas, but to provide otology researchers with guidance concerning the best choice of animal model according to their area of interest. This study described and compared the sizes of the middle and inner ear structures between humans, guinea pigs, gerbils, rats, and mice by micro-CT imaging. The 3D representations obtained provide a better visualization of each element and its accessibility (tympanic membrane, ossicular chain, and cochlea). While prior studies have examined rodent ear morphometry, fewer have focused on their relevance to human medicine [10–12]. The choice of species for studies has generally been based primarily on the habits of researchers and availability rather than specific anatomic considerations [13–16]. This article provides guidance for the selection of the most appropriate rodent study model according to the structure considered (Figure 5).

4.1 | Middle Ear Pathology

4.1.1 | Tympanic Membrane Manipulation

The dimensions of the external auditory canal are crucial for access to the tympanic membrane but have been insufficiently documented in the literature [1, 17]. This information is essential for manipulations involving the tympanic membrane: a diameter of 2 mm can accommodate the smallest pediatric speculum, but at diameters of less than 3 mm, introducing micro-instruments while maintaining a clear view of the tympanic membrane is challenging. Rats and mice therefore present certain challenges for in vivo tympanic membrane manipulation, particularly given the limited

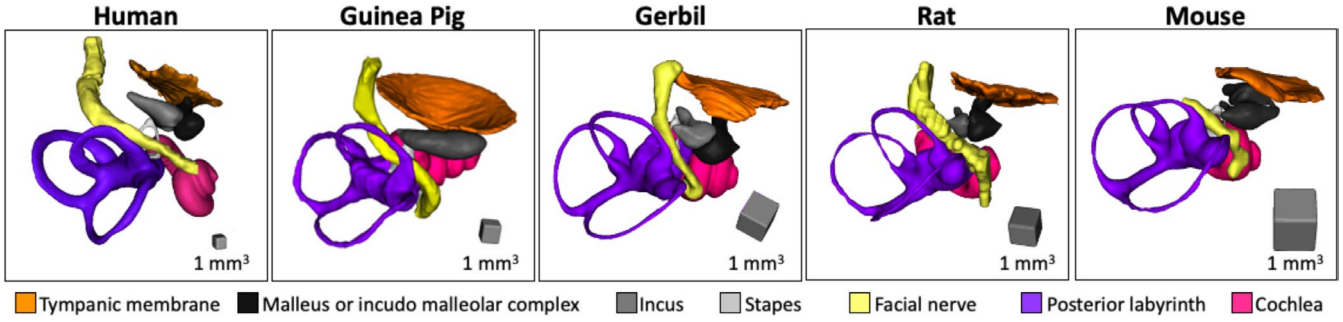

FIGURE 4 | Semicircular canals from humans and rodents: 3D reconstruction of the middle and inner ears.

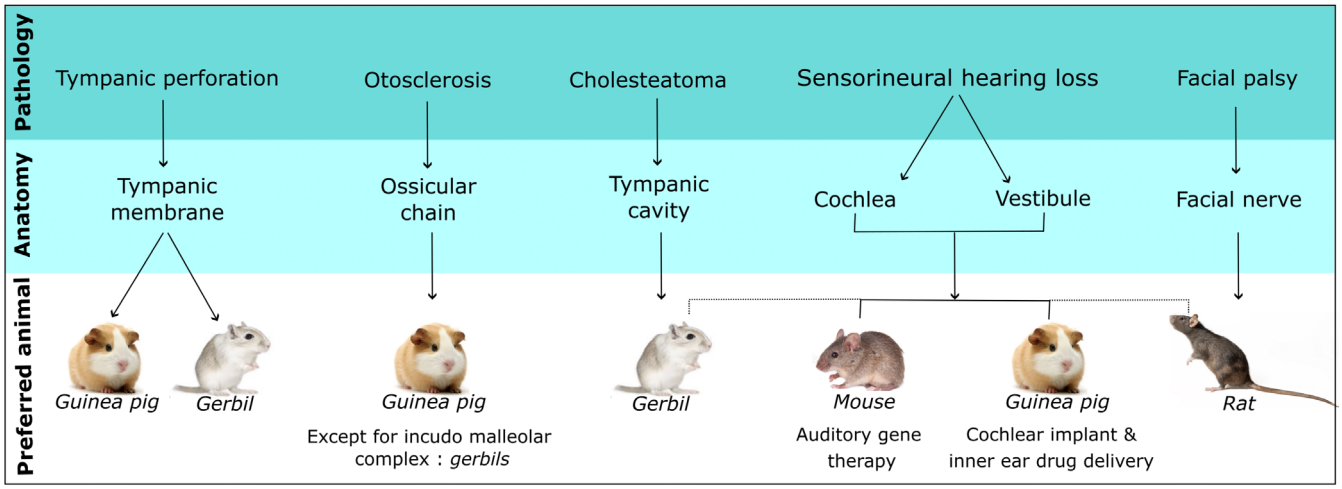

FIGURE 5 | Most appropriate animal models for studies of various otological conditions.

area of the tympanic membrane visible (34%–47%). On the other hand, the external auditory canal is widest in guinea pigs, facilitating access to the tympanic membrane. However, even in guinea pigs, as with other rodents, only the upper portion of the tympanic membrane is well visualized, with the lower part remaining inaccessible via the external auditory canal. While one might assume that guinea pigs are the most commonly used animals for studies on the tympanic membrane, it is actually the rat that seems to be the most widely used among rodents for tympanic membrane manipulations, typically utilizing otomicroscopic or endoscopic evaluation [18–22]. A few studies involving mice were also described, generally involving the posterior superior quadrant of the tympanic membrane [23–25]. Despite the guinea pig advantages, probably due to factors such as greater availability, lower cost, established research protocols, and a historical preference in biomedical research, other rodents seemed to be privileged in tympanic membrane studies.

4.1.2 | Incudo-Malleolar Complex Manipulation

A key element of the anatomy of the incus and malleus in rats and mice is that these two ossicles are fused [1]. This fusion is a distinct anatomic difference relative to humans. Therefore, for investigations involving these ossicles, other species, such as guinea pigs or gerbils, should be preferred. Guinea pigs are especially useful for this purpose, given their larger size, facilitating manipulations of middle ear structures [1, 3, 5, 17, 26].

4.1.3 | Otosclerosis

The possibilities for stapes manipulation are limited for the *Muridae* family (gerbils, rats, and mice) due to the persistence of the stapedial artery [1, 3]. Guinea pigs should therefore be favored for such studies as this species has a stapes about half the size of that in humans and an equivalent structure.

4.1.4 | Cholesteatoma

The $\frac{\text{tympanic cavity volume}}{\text{malleus} + \text{incus} + \text{stapes volume}}$ (×170) ratio was highest in gerbils (Table 1), further attesting to the suitability of this species as a model organism for investigating cholesteatoma pathogenesis. The gerbil is already a recognized model for cholesteatoma research due to its tendency to develop this condition spontaneously, making it the only species other than humans known to do so [27–30]. In fact, the cauterization model of the Auditory Tube described by Wolfman and Chole in 1996, observed the occurrence of pars flaccida retraction and cholesteatoma formation in gerbils [31]. This model has been widely used ever since.

4.2 | Inner Ear Treatment

Mice emerged as the principal model species for the development of animal models of human deafness, following the analysis of their genome. This is a model for which genetic

manipulations are well-established, allowing the reproduction of human deafness conditions [6, 15, 32, 33]. They have been widely and successfully used to explore various aspects of auditory gene therapy [34]. However, they may not constitute an optimal model for certain inner ear studies, as not all applications are based on genetics. Some manipulations may require a larger cochlea, in which it is easier to perform manipulations, with more than 2.5 turns of the cochlea or better access to the scala vestibuli [15]. Guinea pig cochleas, which have 3.5 turns and a volume of ~11 mm^3, have long been known to display physical similarity to the human cochlea [35]. Guinea pigs have, thus, been widely used as an animal model for cochlear implant studies [36–41], investigations of cochlear hair cell regeneration [42], and studies of hearing loss [39], and inner ear drug delivery [34]. The smaller size of the mouse cochlea and rat makes implantation technically challenging and precludes use of human CI electrode arrays. Yet, commercially available electrode arrays have been developed for pre-clinical studies focused on hearing preservation after cochlear implantation, such as the animal array HL03 for mice [43, 44] or HL08 for rats [45] (Cochlear).

4.3 | Facial Nerve Regeneration

Facial expressions have been recognized in various animal species, including guinea pigs, mice, and rats [46]. Rats are an excellent model for investigating facial nerve regeneration because they display positively valenced behavior. This provides a straightforward and dependable readout for measuring functional recovery. Furthermore, rats are particularly suited for facial nerve studies due to their favorable nerve anatomy [16]—specifically, a larger nerve diameter and a relatively superficial anatomical course, which facilitate dissection, surgical manipulation, and post-operative assessments [5].

5 | Conclusion

Micro-CT imaging is an accurate technique that can enhance our knowledge of rodent temporal bone anatomy for otological research. Through comparisons of various rodent species, it can provide crucial insight into the most appropriate model for particular studies based on the specific anatomic features investigated (middle ear, inner ear or facial nerve). This technique can therefore guide researchers, helping them to make informed choices of experimental model and therefore to optimize the translatability of the results to human conditions. Ultimately, the findings of this study not only refine current methodologies in otological research, but also pave the way for more innovative approaches, potentially leading to more appropriate solutions.

Acknowledgments

In vivo imaging was performed at the Life Imaging Facility of Paris University (Plateforme Imageries du Vivant), with support from France Life Imaging (grant ANR-11-INBS-0006) and Infrastructures Biologie-Santé.

Conflicts of Interest

The authors declare no conflicts of interest.

Data Availability Statement

Data sharing not applicable to this article as no datasets were generated or analyzed during the current study.

References

1. A. A. S. Albuquerque, M. Rossato, J. A. A. de Oliveira, and M. A. Hyppolito, "Understanding the Anatomy of Ears From Guinea Pigs and Rats and Its Use in Basic Otologic Research," *Brazilian Journal of Otorhinolaryngology* 75, no. 1 (2009): 43–49, https://doi.org/10.1016/S1808-8694(15)30830-2.

2. A. Schanaider and P. Silva, "The Use of Animals in Experimental Surgery," *Acta Cirúrgica Brasileira* 19 (2004): 441–447, https://doi.org/10.1590/S0102-86502004000400014.

3. R. Asarch, M. Abramson, and W. B. Litton, "Surgical Anatomy of the Guinea Pig Ear," *Annals of Otology, Rhinology, and Laryngology* 84, no. 2 PART 1 (1975): 250–255, https://doi.org/10.1177/000348947508400220.

4. S. Radtke-Schuller, G. Schuller, F. Angenstein, O. S. Grosser, J. Goldschmidt, and E. Budinger, "Brain Atlas of the Mongolian Gerbil (*Meriones unguiculatus*) in CT/MRI-Aided Stereotaxic Coordinates," *Brain Structure and Function* 221, no. Suppl 1 (2016): 1–272, https://doi.org/10.1007/s00429-016-1259-0.

5. R. F. Judkins and H. Li, "Surgical Anatomy of the Rat Middle Ear," *Head and Neck Surgery* 117, no. 5 (1997): 438–447.

6. H. X. Yin, P. Zhang, Z. Wang, et al., "Investigation of Inner Ear Anatomy in Mouse Using X-Ray Phase Contrast Tomography," *Microscopy Research and Technique* 82, no. 7 (2019): 953–960, https://doi.org/10.1002/jemt.23121.

7. M. J. Mason, "Of Mice, Moles and Guinea Pigs: Functional Morphology of the Middle Ear in Living Mammals," *Hearing Research* 301 (2013): 4–18, https://doi.org/10.1016/j.heares.2012.10.004.

8. D. P. Clark and C. T. Badea, "Micro-CT of Rodents: State-of-the-Art and Future Perspectives," *Physica Medica* 30, no. 6 (2014): 619–634, https://doi.org/10.1016/j.ejmp.2014.05.011.

9. M. Risoud, N. X. Bonne, M. Fourdrinier, T. Hubert, and C. Vincent, "Technical Note for Post-Auricular Route Surgery in Mongolian Gerbil," *Hearing Research* 337 (2016): 65–69, https://doi.org/10.1016/j.heares.2016.05.010.

10. F. Fritzsche, W. Maier, and I. Ruf, "Ontogeny of the Malleus in *Mesocricetus auratus* (Mammalia, Rodentia): Systematic and Functional Implications for the Muroid Middle Ear," *Anatomical Record (Hoboken, NJ: 2007)* (2024), https://doi.org/10.1002/ar.25565.

11. M. J. Mason, "Structure and Function of the Mammalian Middle Ear. I: Large Middle Ears in Small Desert Mammals," *Journal of Anatomy* 228, no. 2 (2016): 284–299, https://doi.org/10.1111/joa.12313.

12. C. Pfaff, T. Martin, and I. Ruf, "Bony Labyrinth Morphometry Indicates Locomotor Adaptations in the Squirrel-Related Clade (Rodentia, Mammalia)," *Proceedings of the Royal Society B: Biological Sciences* 282, no. 1809 (2015): 20150744, https://doi.org/10.1098/rspb.2015.0744.

13. I. S. Curthoys, "The Organization of the Horizontal Semicircular Duct, Ampulla and Utricle in the Rat and Guinea Pig," *Acta Oto-Laryngologica* 92 (1981): 323–330, https://doi.org/10.3109/00016488109133268.

14. P. Montes-Lourido, M. Kar, M. Pernia, S. Parida, and S. Sadagopan, "Updates to the Guinea Pig Animal Model for In-Vivo Auditory Neuroscience in the Low-Frequency Hearing Range," *Hearing Research* 424 (2022): 108603, https://doi.org/10.1016/j.heares.2022.108603.

15. K. K. Ohlemiller, S. M. Jones, and K. R. Johnson, "Application of Mouse Models to Research in Hearing and Balance," *Journal of the*

Association for Research in Otolaryngology 17, no. 6 (2016): 493–523, https://doi.org/10.1007/s10162-016-0589-1.

16. S. Rink, H. Bendella, S. M. Akkin, M. Manthou, M. Grosheva, and D. N. Angelov, "Experimental Studies on Facial Nerve Regeneration," *Anatomical Record* 302, no. 8 (2019): 1287–1303, https://doi.org/10.1002/ar.24123.

17. M. Bergin, S. Vlajkovic, P. Bird, and P. Thorne, "Systematic Review of Animal Models of Middle Ear Surgery," *World Journal of Otorhinolaryngology* 3 (2013): 71–88, https://doi.org/10.5319/wjo.v3.i3.71.

18. P. Hong, M. Bance, and P. F. Gratzer, "Repair of Tympanic Membrane Perforation Using Novel Adjuvant Therapies: A Contemporary Review of Experimental and Tissue Engineering Studies," *International Journal of Pediatric Otorhinolaryngology* 77, no. 1 (2013): 3–12, https://doi.org/10.1016/j.ijporl.2012.09.022.

19. A. Rahman, P. Olivius, J. Dirckx, M. Von Unge, and M. Hultcrantz, "Stem Cells and Enhanced Healing of Chronic Tympanic Membrane Perforation," *Acta Oto-Laryngologica* 128, no. 4 (2008): 352–359, https://doi.org/10.1080/00016480701762508.

20. H. Seonwoo, S. W. Kim, J. Kim, et al., "Regeneration of Chronic Tympanic Membrane Perforation Using an EGF-Releasing Chitosan Patch," *Tissue Engineering. Part A* 19, no. 17–18 (2013): 2097–2107, https://doi.org/10.1089/ten.TEA.2012.0617.

21. A. Y. Wang, Y. Shen, L. J. Liew, et al., "Rat Model of Chronic Tympanic Membrane Perforation: Ventilation Tube With Mitomycin C and Dexamethasone," *International Journal of Pediatric Otorhinolaryngology* 80 (2016): 61–68, https://doi.org/10.1016/j.ijporl.2015.11.010.

22. A. Y. Wang, Y. Shen, J. T. Wang, P. L. Friedland, M. D. Atlas, and R. J. Dilley, "Animal Models of Chronic Tympanic Membrane Perforation: A "Time-Out" to Review Evidence and Standardize Design," *International Journal of Pediatric Otorhinolaryngology* 78, no. 12 (2014): 2048–2055, https://doi.org/10.1016/j.ijporl.2014.10.007.

23. S. El-Saied, A. Amar, D. M. Kaplan, et al., "Local Alpha1-Antitrypsin Accelerates the Healing of Tympanic Membrane Perforation in Mice," *Laryngoscope* 134, no. 8 (2024): 3802–3806, https://doi.org/10.1002/lary.31454.

24. J. Li, P. O. Eriksson, A. Hansson, S. Hellström, and T. Ny, "Plasmin/Plasminogen Is Essential for the Healing of Tympanic Membrane Perforations," *Thrombosis and Haemostasis* 96, no. 4 (2006): 512–519.

25. Y. Shen, Y. Guo, C. Du, M. Wilczynska, S. Hellström, and T. Ny, "Mice Deficient in Urokinase-Type Plasminogen Activator Have Delayed Healing of Tympanic Membrane Perforations," *PLoS One* 7, no. 12 (2012): e51303, https://doi.org/10.1371/journal.pone.0051303.

26. W. F. Decraemer, O. de La Rochefoucauld, W. R. J. Funnell, and E. S. Olson, "Three-Dimensional Vibration of the Malleus and Incus in the Living Gerbil," *Journal of the Association for Research in Otolaryngology* 15, no. 4 (2014): 483–510, https://doi.org/10.1007/s10162-014-0452-1.

27. M. D. McGinn, R. A. Chole, and K. R. Henry, "Cholesteatoma Induction. Consequences of External Auditory Canal Ligation in Gerbils, Cats, Hamsters, Guinea Pigs, Mice and Rats," *Acta Oto-Laryngologica* 97, no. 3–4 (1984): 297–304, https://doi.org/10.3109/00016488409130992.

28. R. A. Chole, K. R. Henry, and M. D. McGinn, "Cholesteatoma: Spontaneous Occurrence in the Mongolian Gerbil Meriones Unguiculatis," *American Journal of Otology* 2, no. 3 (1981): 204–210.

29. G. Choufani, N. Roper, C. Delbrouck, S. Hassid, and H. J. Gabius, "Animal Model for Cholesteatoma Induced in the Gerbil: Will the Profiles of Differentiation/Growth-Regulatory Markers Be Similar to the Clinical Situation?," *Laryngoscope* 117, no. 4 (2007): 706–711, https://doi.org/10.1097/mlg.0b013e318031d09d.

30. F. C. da Huve, J. A. Bauer, F. A. Selaimen, M. N. L. da Silva, and S. S. da Costa, "Experimental Cholesteatoma: A Comparison Between Spontaneous and Induced Models," *Brazilian Journal of Otorhinolaryngology* 89, no. 1 (2021): 73–78, https://doi.org/10.1016/j.bjorl.2021.09.003.

31. D. E. Wolfman and R. A. Chole, "Experimental Retraction Pocket Cholesteatoma," *Annals of Otology, Rhinology, and Laryngology* 95, no. 6 (1986): 639–644, https://doi.org/10.1177/000348948609500619.

32. S. Early, E. Du, E. Boussaty, and R. Friedman, "Genetics of Noise-Induced Hearing Loss in the Mouse Model," *Hearing Research* 425 (2022): 108505, https://doi.org/10.1016/j.heares.2022.108505.

33. J. A. N. Buytaert, S. B. Johnson, M. Dierick, W. H. M. Salih, and P. A. Santi, "MicroCT Versus sTSLIM 3D Imaging of the Mouse Cochlea," *Journal of Histochemistry and Cytochemistry* 61, no. 5 (2013): 382–395, https://doi.org/10.1369/0022155413478613.

34. G. Lahlou, C. Calvet, M. Giorgi, M. J. Lecomte, and S. Safieddine, "Towards the Clinical Application of Gene Therapy for Genetic Inner Ear Diseases," *Journal of Clinical Medicine* 12, no. 3 (2023): 1046, https://doi.org/10.3390/jcm12031046.

35. B. Liu, X. L. Gao, H. X. Yin, S. Q. Luo, and J. Lu, "A Detailed 3D Model of the Guinea Pig Cochlea," *Brain Structure & Function* 212, no. 2 (2007): 223–230, https://doi.org/10.1007/s00429-007-0146-0.

36. J. S. C. de Andrade, P. Baumhoff, O. L. M. Cruz, T. Lenarz, and A. Kral, "Cochlear Implantation in an Animal Model Documents Cochlear Damage at the Tip of the Implant," *Brazilian Journal of Otorhinolaryngology* 88, no. 4 (2022): 546–555, https://doi.org/10.1016/j.bjorl.2020.07.017.

37. M. Drouillard, R. Torres, E. Mamelle, et al., "Influence of Electrode Array Stiffness and Diameter on Hearing in Cochlear Implanted Guinea Pig," *PLoS One* 12, no. 8 (2017): e0183674, https://doi.org/10.1371/journal.pone.0183674.

38. N. El Kechai, E. Mamelle, Y. Nguyen, et al., "Hyaluronic Acid Liposomal Gel Sustains Delivery of a Corticoid to the Inner Ear," *Journal of Controlled Release* 226 (2016): 248–257, https://doi.org/10.1016/j.jconrel.2016.02.013.

39. R. D. Frisina, M. Budzevich, X. Zhu, G. V. Martinez, J. P. Walton, and D. A. Borkholder, "Animal Model Studies Yield Translational Solutions for Cochlear Drug Delivery," *Hearing Research* 368 (2018): 67–74, https://doi.org/10.1016/j.heares.2018.05.002.

40. C. Jaudoin, F. Agnely, Y. Nguyen, E. Ferrary, and A. Bochot, "Nanocarriers for Drug Delivery to the Inner Ear: Physicochemical Key Parameters, Biodistribution, Safety and Efficacy," *International Journal of Pharmaceutics* 592 (2021): 120038, https://doi.org/10.1016/j.ijpharm.2020.120038.

41. E. Mamelle, N. El Kechai, V. Adenis, et al., "Assessment of the Efficacy of a Local Steroid Rescue Treatment Administered 2 Days After a Moderate Noise-Induced Trauma in Guinea Pig," *Acta Oto-Laryngologica* 138, no. 7 (2018): 610–616, https://doi.org/10.1080/00016489.2018.1438659.

42. P. J. Atkinson, A. K. Wise, B. O. Flynn, B. A. Nayagam, and R. T. Richardson, "Hair Cell Regeneration After ATOH1 Gene Therapy in the Cochlea of Profoundly Deaf Adult Guinea Pigs," *PLoS One* 9, no. 7 (2014): e102077, https://doi.org/10.1371/journal.pone.0102077.

43. A. D. Claussen, R. Vielman Quevedo, B. Mostaert, J. R. Kirk, W. F. Dueck, and M. R. Hansen, "A Mouse Model of Cochlear Implantation With Chronic Electric Stimulation," *PLoS One* 14, no. 4 (2019): e0215407, https://doi.org/10.1371/journal.pone.0215407.

44. D. J. Colesa, J. Devare, D. L. Swiderski, L. A. Beyer, Y. Raphael, and B. E. Pfingst, "Development of a Chronically-Implanted Mouse Model for Studies of Cochlear Health and Implant Function," *Hearing Research* 404 (2021): 108216, https://doi.org/10.1016/j.heares.2021.108216.

45. L. A. J. Reiss, J. Kirk, A. D. Claussen, and J. B. Fallon, "Animal Models of Hearing Loss After Cochlear Implantation and Electrical Stimulation," *Hearing Research* 426 (2022): 108624, https://doi.org/10.1016/j.heares.2022.108624.

46. K. Finlayson, J. F. Lampe, S. Hintze, H. Würbel, and L. Melotti, "Facial Indicators of Positive Emotions in Rats," *PLoS One* 11, no. 11 (2016): e0166446, https://doi.org/10.1371/journal.pone.0166446.

Supporting Information

Additional supporting information can be found online in the Supporting Information section.